

The self-actuating InAs nanowire-based nanoelectromechanical Josephson junction

Andrey V. Kretinin,^{1,*} Anindya Das,¹ and Hadas Shtrikman¹

¹*Weizmann Institute of Science, Condensed Matter Physics Department, Rehovot, Israel*

Half a century ago Brian Josephson made a series of striking predictions related to a tunnelling barrier sandwiched between two superconductors.¹ One particular prediction, later became known as the a.c.-Josephson effect, said that under a finite d.c. bias the tunnelling current contains an a.c. supercurrent component, oscillating at microwave frequency. This prediction was experimentally verified through observation of the junction current-voltage characteristics modified by the interaction with the electromagnetic radiation,^{2,3} and direct detection of the microwave radiation emitted from the junction itself.⁴ It had also been established that the behaviour of the d.c. current-voltage characteristic is determined by the high-frequency dynamics of the Josephson junction,⁵ and can be used to study various systems such as atoms in the electron-spin resonance,⁶ optical phonons in high- T_c superconductors,⁷ and vibrating Nb molecules.⁸ Here we present an InAs nanowire Josephson junction device,^{9,10} where a vibrating nanowire weak link plays the role of a nanoelectromechanical resonator. The flow of the a.c.-Josephson current through the junction enabled actuation and detection of vibrational modes of the resonator by means of simple d.c. transport measurements.

There are two regimes a Josephson junction can be operated in.¹ The first, the so-called d.c.-Josephson effect, is characterised by a d.c. superconducting current $I_s = I_c \sin(\Delta\phi)$, where I_c is the critical current, and $\Delta\phi$ is the superconducting wave functions phase difference. In the second regime corresponding to the a.c.-Josephson effect the tunnelling current exceeds the value of I_c , and consists of two components. Apart from a normal dissipative current manifested by the voltage drop V , the total current contains the oscillating superconductive part $I_s = I_c \sin(\omega_j t + \phi_0)$, where ϕ_0 is the initial phase difference. In this case the phase difference increases linearly in time t with the rate set by the d.c. voltage as $\omega_j = (2e/\hbar)V$.

Because of the high frequency of the a.c.-Josephson current ($2e/h \approx 483.6$ MHz/ μ V), the shape of the Josephson junction current-voltage ($I - V$) characteristics is determined by its electrical impedance.^{3,5} One of the most vivid demonstrations of this fact was the experiment of Coon and Fiske,³ where the $I - V$ characteristics of the Josephson junction coupled to the electromagnetic resonator, exhibited constant-voltage step features (self-induced Shapiro steps). In this experiment the steps occurred when the voltage V was such that the

a.c.-Josephson oscillations were in resonance, namely, at voltage $V_n = \hbar\omega_n/2e$, where ω_n is the frequency of the n -th resonator mode. This work illustrated how a Josephson junction coupled to an external resonant system can be simultaneously used as a source and detector of the microwave radiation. This remarkable property allowed the use of a Josephson junction as an ultra-small power spectrometer to study atomic and vibrational spectra.⁶⁻⁸

Recently, the combination of the Josephson junction and nanoelectromechanical system¹¹ (NEMS) has attracted increasing attention. It was proposed to use the nanomechanical resonator to store the Josephson junction phase qubit states,^{12,13} and to build a coherent source of microwave radiation based on an array of Josephson junctions.¹⁴ In addition, a vibration-modulated Josephson junction has been predicted to exhibit self-induced Shapiro steps in the $I - V$ characteristics at a frequency of mechanical resonance,¹⁵ and the weak-link made of a doubly-clamped nanowire can be used to pump the supercurrent into nanowire vibrations.¹⁶ In all these aspects NEMS act similarly to an external microwave resonator coupled to a Josephson junction.

Here we report observation of the a.c.-Josephson oscillations being in resonance with the longitudinal acoustic wave of an InAs nanowire. Using a previously developed technique¹⁷ we fabricated a new type of nanowire Josephson junction device^{9,10} (Figs. 1a and 1b). In our field-effect type device the 240 nm-long nanowire weak-link is suspended in vacuum and clamped by two superconducting Ti/Al contacts, making the nanowire-based NEMS¹⁸ an integral part of the Josephson junction. The transport experiments with the current-driven Josephson junction described here were carried out inside the dilution refrigerator with $T_{\text{base}} \approx 15$ mK. All measurements were taken at a fixed voltage on the local and global backgates. Figure 1c shows the experimental $I - V$ curve typical of an underdamped Josephson junction; a non-dissipative branch limited by the critical current $I_c \approx 6.5$ nA, some hysteresis at around I_c , and the resistive part, with the well-pronounced step-like features. To look into the details of the $I - V$ curve we measured the differential resistance dV/dI as a function of applied voltage V (Fig. 1d). At the subgap voltages ($e|V| < 2\Delta$, here 2Δ is the superconducting gap in the Al contacts) the differential resistance reveals an overall decrease with some dips originating from the excess current of the so-called Multiple Andreev Reflections¹⁹ (MAR). The dips in the resistance occur when the superconducting gap 2Δ is an integer multiple of the applied bias, which defines the position of the MAR signature as $V_m = \pm 2\Delta/em$, where m is integer. In our experi-

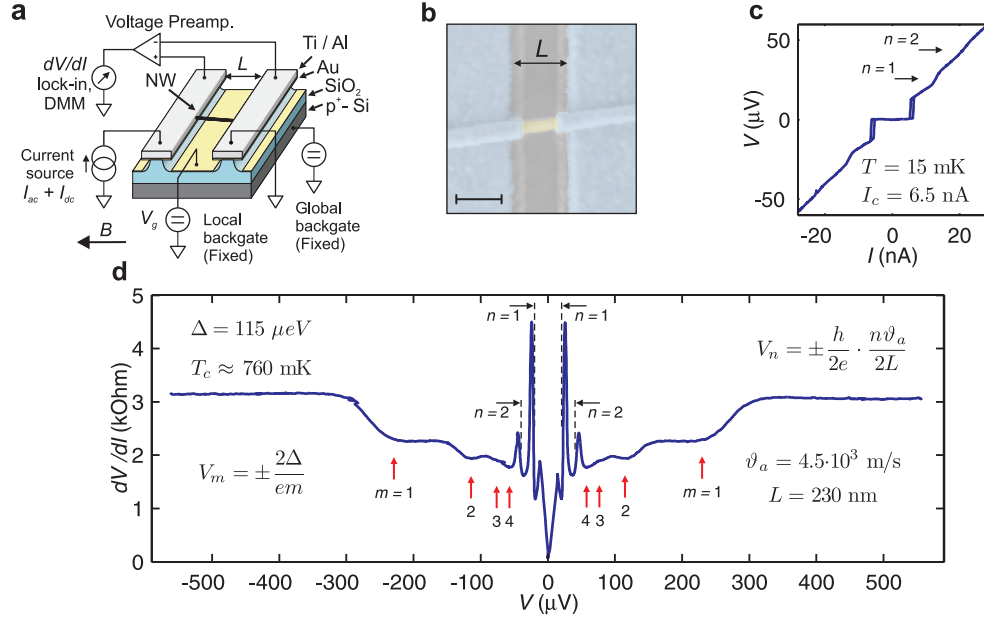


FIG. 1. **The suspended InAs nanowire-based Josephson junction and its $I - V$ characteristics.** (a) A schematic representation of the suspended nanowire device and the experimental set-up. The InAs nanowire (NW) is suspended over a trench predefined in SiO_2 , and clamped by two Ti/Al contacts. An in-plane magnetic field B was applied during the experiment, and it was only few degrees off the nanowire axis. (b) The top view of a typical device obtained by a scanning electron microscope. The scale bar is 200 nm. The fake colours indicate different parts of the device. Blue is the Ti/Al contacts, yellow is the nanowire, and gray is the local backgate below the nanowire. (c) The $I - V$ characteristics of the nanowire Josephson junction taken at $V_g = 12.3$ V. (d) The differential resistance dV/dI as a function of the voltage V taken at the same V_g as in (c). The red arrows show first four orders of MAR at voltage V_m . The position of the first MAR signature ($m = 1$) gives the superconducting gap $2\Delta \approx 230$ μeV and the estimate for $T_c \approx 2\Delta/(3.52 k_B) \approx 760$ mK. The black arrows mark the resistance resonances caused by the acoustic wave actuated by Josephson oscillations at voltage V_n .

ment we clearly observed MAR signatures with m up to four (red arrows in Fig. 1d). However, at lower biases, the subgap features become sharp well-recognised asymmetric resistance resonances (black arrows in Fig. 1d), corresponding to the steps on the $I - V$ curve (Fig. 1c). The distinct nature of these resonances becomes apparent from the gray-scale plot of dV/dI measured at different magnetic fields shown in Fig. 2a. The position of the MAR signatures is tightly bound to the value of the magnetic field- and temperature-dependent gap 2Δ , and shifts toward $V = 0$ as the magnetic field B , or temperature T , approach their critical values. As seen from Fig. 2a, the position of the MAR signatures for $m = 1, 2$ follow the prediction of the Landau-Ginzburg theory²⁰ (red dashed curves). Whereas, the position of the resistance resonances (black arrows) remains unchanged, and the resonances simply vanish for $B \geq B_c$. Qualitatively the same behaviour is observed for dV/dI measured at different temperatures. Moreover, the position of the resonances is independent of the backgate voltage V_g (Fig. 2b), which rules out the superconducting bound states^{21,22} as possible explanation for their origin.

Such a peculiar behaviour indicates that these features are due to the self-induced Shapiro steps of the junction coupled to an external resonator.²³ The first resonance appears at around $V \approx 20$ μV , which corresponds to an

a.c.-Josephson frequency of about 10 GHz. In our experiment there was no deliberately designed microwave resonator coupled to the nanowire junction. The possibility of a microwave cavity unintentionally formed inside our cryogenic setup was excluded by reproducing the same result in a different cryogenic system. The distributed parameter resonators, such as coplanar striplines, are ruled out by the fact that the dimensions of the device including the leads do not exceed 1 mm, and it is much smaller than the radiation wavelength (~ 3 cm). We also considered a lumped LC circuit, where the capacitance is defined by the area of the device bonding pads (~ 3 pF), and the inductance is defined by the device leads (~ 1 nH). The estimated resonant frequency (~ 3 GHz) appears to be well below the measured one.

The important clue to the understanding of the observed resistance resonances lies in the fact that the nanowire junction is suspended and its possible mechanical oscillations are not damped by the substrate. Indeed, a quick estimation shows that the a.c.-Josephson frequency of the resonances turn out to be close to the frequency of the first two longitudinal acoustic modes of the doubly-clamped InAs beam²⁴ $f_n = (\vartheta_a/2L) \times n \approx 9.4$ GHz $\times n$, where n - is integer, $\vartheta_a = 4.5 \times 10^3$ m/s is the speed of sound in wurtzite InAs nanowire along the $\langle 111 \rangle$ direction,²⁵ and $L = 240$ nm is the length of the

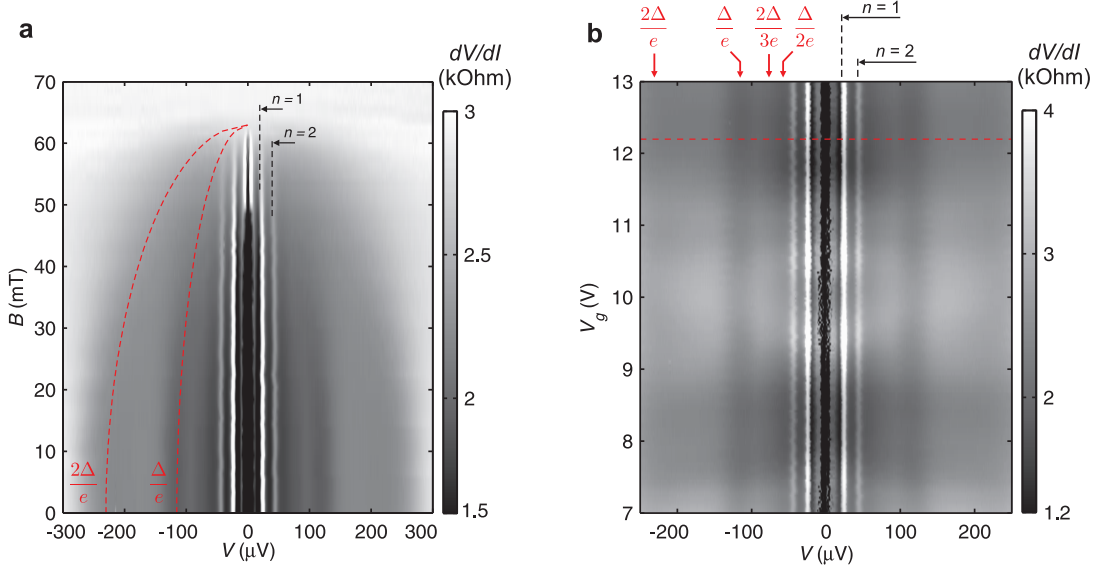


FIG. 2. **The magnetic field- and gate voltage-independent position of the resistance resonances.** (a) The gray-scale plot of dV/dI made in the $V - B$ plane at $T = T_{\text{base}}$. The red dashed curves show the position of the first two orders of MAR expected from the Landau-Ginzburg theory,²⁰ $\Delta(B)/\Delta(0) = \sqrt{1 - (B/B_c)^2}$, where $B_c = 63$ mT is the critical field. The black arrows mark the magnetic field-independent position of the resistance resonances. The position of the resistance resonances stays unchanged while the peak amplitude decreases while B approaches its critical values B_c . (b) The gray-scale plot of dV/dI made in the $V - V_g$ plane at the same temperature as in (a). The red arrows point at the first four MAR signatures seen in Fig. 1d. The black arrows show the gate voltage-independent resistance resonances. The horizontal red dashed line marks the dV/dI trace shown in Fig. 1d taken at $V_g = 12.3$ V. The changing shades of gray quasi-periodic in V_g are due to the Fabry-Pérot quasiparticle conductance oscillations.¹⁷

beam. This suggests that the resistance resonances are caused by interaction of the a.c.-Josephson current with the acoustic modes of the nanowire. Since the mode frequency is defined only by the nanowire length the position of the resonances caused by them should be independent of the values of Δ and V_g , which is confirmed by our observations.

To further understand this phenomenon we used a simple model of the Josephson junction coupled to an InAs nanowire-based Bulk Acoustic Resonator²⁶ (BAR).

The junction is described by the RSJ-model⁵ (Fig. 3a), where an ideal junction J is connected in parallel to the normal state resistance R_n , and the total junction capacitance C_j . As mentioned before, the shape of the $I - V$ characteristics is governed by the high-frequency properties of the junction, namely by the relative impedance of R_n and C_j , and characterised by the parameter $\beta = \omega_c R_n C_j$,⁵ where $\omega_c = (2e/\hbar)I_c R_n$ is the lowest frequency of the Josephson oscillations. If C_j is large ($\beta \gg 1$) the junction is ‘underdamped’ and the $I - V$ curve is linear. In the opposite limit of small C_j ($\beta \ll 1$), the junction is ‘overdamped’ and the $I - V$ curve is parabolic. The experimental values of the critical current ($I_c = 6.5$ nA) and the normal-state resistance ($R_n \sim 2$ kOhm) gave us the lowest value of the Josephson oscillations frequency $\omega_c/2\pi \sim 6.3$ GHz, and $\beta \approx 30$ (with $C_j \sim 3$ pF), indicating that the junction is ‘underdamped’.

In our device capacitance C_j is a result of the parallel

connection of the leads capacitance and the piezoelectric capacitor formed by the wurtzite InAs nanowire.²⁷ In the case of a piezoelectric capacitor the external a.c. electric field excites acoustic waves inside the dielectric media and vice versa. The process of energy conversion from the electrical to the mechanical domain profoundly affects the capacitor impedance, and is the basis of the BAR operation. According to the one-dimensional Mason model²⁶ the total effective impedance $Z_e(\omega)$ of a piezoelectric capacitor is

$$Z_e(\omega) = \frac{1}{j\omega C_j} \left[1 - k_t^2 \cdot \frac{\tan\left(\frac{\omega L}{2v_a}\right)}{\frac{\omega L}{2v_a}} \right], \quad (1)$$

where ω is the angular frequency, k_t^2 is the piezoelectric coupling constant, v_a is the speed of sound in the piezoelectric media, and L is the thickness of the piezoelectric material. It is clear from Eq. (1) that the longitudinal acoustic standing wave with $\omega_r = (\pi/L)v_a$ causes the total impedance to diverge ($Z_e(\omega_r) \rightarrow \infty$).

Now we assume that instead of C_j the Josephson junction dynamics is defined by the impedance Z_e of the InAs nanowire BAR (Fig. 3b). While the BAR is off resonance, the $I - V$ curve follows the one expected for the underdamped regime (blue curve, Fig. 3c). When the voltage V is such that the Josephson oscillations are in resonance with the BAR its impedance increases, forcing the Josephson junction to cross from the underdamped to the

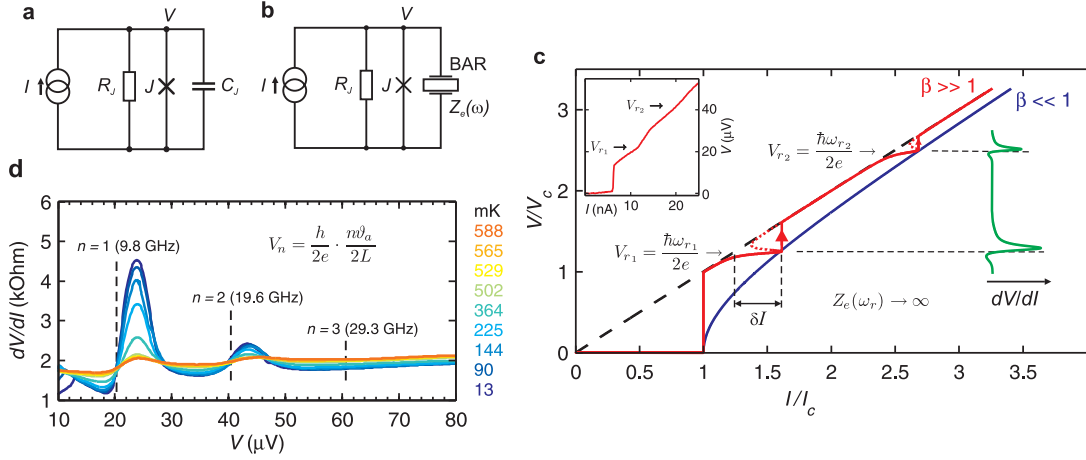


FIG. 3. The RSJ-model and $I - V$ characteristics of the Josephson junction coupled to the Bulk Acoustic Resonator. (a) The RSJ-model circuit diagram of a typical Josephson junction. (b) The RSJ-model of the Josephson junction coupled to the BAR. (c) The schematic plot of the Josephson junction $I - V$ characteristics. If the capacitance C_J is large ($\beta \gg 1$) the a.c.-Josephson current is shunted by C_J , and its time-averaged contribution to the $I - V$ characteristics is zero. Thus for $I > I_c$ the $I - V$ characteristics is of a normal conductor $V = IR_n$ (black dashed line). In the opposite case of small C_J ($\beta \ll 1$) the alternating current is forced to flow through R_n causing the a.c.-Josephson current to be frequency-modulated. The time-average of the frequency-modulated a.c. current is non-zero, which makes the total $I - V$ characteristics parabolic⁵ $V/V_c = \sqrt{(I/I_c)^2 - 1}$, where $V_c = R_n I_c$ (blue curve). The $I - V$ characteristics of the underdamped Josephson junction coupled to the BAR is shown by the red curve. When the voltage $V = V_r$ the Josephson oscillations actuate the acoustic resonance in BAR ($Z_e(\omega) \rightarrow \infty$), which forces the junction to cross from the underdamped to the overdamped regime, and results in the current peak δI . For simplicity we assumed that the resonance in Z_e has a Lorentzian lineshape. In the case of the current-driven junction, the current peak takes a step-like shape with a multi-valued region showed by the red dotted curve. The green curve on the right-hand side is the corresponding dV/dI as a function of V . (Inset) The actual $I - V$ curve measured at $T = T_{\text{base}}$ and $B = 0$. (d) The zoomed-in plot of the dV/dI resonance taken at different temperatures and zero magnetic field. Identically to the magnetic field dependence (Fig. 2a), the position of the resonances is independent of the temperature, which rules out their MAR-related origin. We used the interception point of curves taken at different T to identify the resonant voltage V_n . The vertical dashed lines designate the voltage V_n which corresponds to the first three longitudinal harmonics expected for the doubly-clamped InAs beam with length $L = 230$ nm and speed of sound $v_a = 4.5 \cdot 10^3$ m/s. The respective frequencies are given in brackets.

overdamped regime (red curve, Fig. 3c). This crossing results in a cusp-like increase of the d.c.-current through the junction δI with the maximum at $V_r = \hbar\omega_r/2e$, where ω_r is the mechanical resonance frequency. In the case of the current-driven Josephson junction the current peak on the $I - V$ curve becomes a step-like feature and corresponds to the asymmetric resonance in dV/dI (green curve, Fig. 3c).

Using this model, we determined the resonant frequency of the nanowire BAR actuated by the Josephson oscillations. Two resistance peaks shown in Fig. 3d correspond to the resonant coupling of the first two longitudinal acoustic modes of the doubly-clamped InAs nanowire,²⁴ with onset at the voltage determined as

$$V_n = \pm \frac{\hbar\omega_r}{2e} = \pm \frac{\hbar}{2e} \cdot \frac{n v_a}{2L^*},$$

where $n = 1, 2$ and $L^* = 230$ nm is the length of the acoustic resonator ($v_a = 4.5 \times 10^3$ m/s). Note, the length of the resonator L^* found here is close to the physical length of the nanowire Josephson junction (240 nm). Despite the fact that the resonance in Z_e requires a non-zero spatially averaged strain,²⁶ which forbids the appearance

of even harmonics, we have observed the second harmonic as well. The reason for that is the slightly asymmetric geometry of our device.

The piezoelectric coupling of the Josephson oscillations to the acoustic mode of a crystal resonator has been theoretically studied for the case of an array of Josephson junctions.¹⁴ From this point of view our experimental realisation can be seen as a special case of a single weakly coupled junction. Other possible coupling mechanisms such as the magnetomotive force,¹⁶ and modulation of the junction dimensions¹⁵ are ruled out since the resonance is observed at $B = 0$, and the junction length L is fixed. It is worth mentioning that the strong coupling between the longitudinal vibrations and single charge tunneling by means of electron-vibron coupling²⁸ has been observed in suspended carbon nanotubes.^{29,30} However, the underlying physical principals responsible for the electron-vibron coupling is entirely different from the one studied in this work.

In conclusion, we fabricated an InAs nanowire nanoelectromechanical Josephson junction, and observed the resonant coupling of Josephson oscillations to the longitudinal acoustic modes of the nanowire. The reso-

nant coupling reveals itself as voltage steps in the junction $I - V$ characteristics occurring when the Josephson oscillations are in resonance with the acoustic modes. We showed that the Josephson junction coupled to the NEMS can be used as a self-actuating probe to study vibrational states. The advantage of this tool is in its simplicity, the NEMS is probed by routine d.c.-measurements, with no need for external high-frequency equipment.^{11,13,18} Also, our experiment demonstrates the possibility of building a nano-scale source of coherent microwave radiation based on an array of Josephson junctions coupled to a high- Q piezoelectric resonator.¹⁴

METHODS – The high-quality InAs nanowires used in this work have been synthesised by the Molecular-Beam Epitaxy in Riber 32 solid source system by the Au-assisted Vapour-Liquid-Solid (VLS) method. The nanowires were grown along $\langle 111 \rangle$ direction on a (011)-oriented InAs substrate at 400 °C and the group V/III ratio of 100. All nanowires have a pure wurtzite crystal structure with only one stacking fault per several nanowires.¹⁷

The basis of the suspended nanowire Josephson junction was a p⁺-Si wafer with 300 nm thick SiO₂ thermally grown on top. First, an array of 250 nm \times 20 μ m trenches was chemically etched in the SiO₂ to depth of about 150 nm. This was followed by evaporation of the local metal backgate on the bottom of the trenches. Then nanowires were randomly distributed across the predefined trenches so that a small segment of a nanowire is suspended over the trench. E-beam lithography was employed to pattern Ti/Al contacts (5 nm/100 nm) on top of the parts of the nanowire supported by the banks of the trench, leaving the suspended segment un-

touched (Fig 1a). To ensure high contact transparency the nanowire native oxide was removed with the 0.2% solution of (NH₄)₂S_x ($x = 1.5$ M) prior to evaporation of the contacts. The nanowire junction was about 240 nm long with a diameter of about 50 nm (Fig 1b). The experimental data obtained from another device is given in the Supplementary Information.

All transport measurements were carried out inside a ³He-⁴He dilution refrigerator with heavily filtered signal lines and $T_{\text{base}} \approx 15$ mK. The $I - V$ characteristics and differential resistance as a function of d.c. voltage were measured in a quasi four-terminal constant current configuration. The voltage drop across the device was amplified with a low-noise voltage preamplifier and registered using a high-speed digital voltmeter or lock-in amplifier (Fig. 1a). The a.c. excitation current I_{ac} was set to be below 400 pArms, so that the excitation voltage drop across the sample was not greater than $k_{\text{B}}T$.

ACKNOWLEDGMENTS – Authors would like to acknowledge Moty Heiblum for making this project possible, and for critical remarks and comments made during the work. The authors are grateful to Eli Zeldov and David Stroud for the enlightening discussions. We also would like to thank Denis Vasyukov, Yuval Oreg, Alex Palevskii for sharing their knowledge of superconductivity, Yunchul Chung for technical ideas, Diana Mahalu for the expertise in e-beam lithography and Ronit Popovitz-Biro for professional TEM study of the InAs nanowires. This work was partially supported by the EU FP6 Program Grant No. 506095, by the Israeli Science Foundation Grant No. 530-08, and Israeli Ministry of Science Grant No. 3-66799.

* andrey.kretinin@manchester.ac.uk

¹ Josephson, B. Possible new effects in superconductive tunnelling. *Phys. Lett.* **1**, 251–253 (1962).

² Shapiro, S. Josephson Currents in Superconducting Tunneling: The Effect of Microwaves and Other Observations. *Phys. Rev. Lett.* **11**, 80–82 (1963).

³ Coon, D. D. & Fiske, M. D. Josephson ac and Step Structure in the Supercurrent Tunneling Characteristic. *Phys. Rev.* **138**, A744–A746 (1965).

⁴ Yanson, I., Svistunov, V. & Dmitrenko, I. Experimental observation of tunnel effect for Cooper pairs with emission of photons. *Sov. Phys. JETP* **21**, 650 (1965).

⁵ McCumber, D. E. Effect of ac Impedance on dc Voltage-Current Characteristics of Superconductor Weak-Link Junctions. *J. Appl. Phys.* **39**, 3113–3118 (1968).

⁶ Baberschke, K., Bures, K. D. & Barnes, S. E. ESR in *Situ* with a Josephson Tunnel Junction. *Phys. Rev. Lett.* **53**, 98–101 (1984).

⁷ Helm, C. *et al.* Coupling between Phonons and Intrinsic Josephson Oscillations in Cuprate Superconductors. *Phys. Rev. Lett.* **79**, 737–740 (1997).

⁸ Marchenkov, A., Dai, Z., Donehoo, B., Barnett, R. N. & Landman, U. Alternating current Josephson effect and

resonant superconducting transport through vibrating Nb nanowires. *Nat. Nano* **2**, 481–485 (2007).

⁹ Doh, Y.-J. *et al.* Tunable Supercurrent Through Semiconductor Nanowires. *Science* **309**, 272–275 (2005).

¹⁰ Xiang, J., Vidan, A., Tinkham, M., Westervelt, R. M. & Lieber, C. M. Ge/Si nanowire mesoscopic Josephson junctions. *Nat. Nano* **1**, 208–213 (2006).

¹¹ Ekinici, K. L. & Roukes, M. L. Nanoelectromechanical systems. *Rev. Sci. Instrum.* **76**, 061101 (2005).

¹² Cleland, A. N. & Geller, M. R. Superconducting Qubit Storage and Entanglement with Nanomechanical Resonators. *Phys. Rev. Lett.* **93**, 070501 (2004).

¹³ O’Connell, A. D. *et al.* Quantum ground state and single-phonon control of a mechanical resonator. *Nature* **464**, 697–703 (2010).

¹⁴ Trees, B. R., Natu, S. & Stroud, D. Nanomechanical-resonator-induced synchronization in Josephson junction arrays. *Phys. Rev. B* **72**, 214524 (2005).

¹⁵ Zhu, J.-X., Nussinov, Z. & Balatsky, A. V. Vibration-mode-induced Shapiro steps and back action in Josephson junctions. *Phys. Rev. B* **73**, 064513 (2006).

¹⁶ Sonne, G., Shekhter, R. I., Gorelik, L. Y., Kulinich, S. I. & Jonson, M. Superconducting pumping of nanomechanical

- vibrations. *Phys. Rev. B* **78**, 144501 (2008).
- ¹⁷ Kretinin, A. V., Popovitz-Biro, R., Mahalu, D. & Shtrikman, H. Multimode Fabry-Pérot Conductance Oscillations in Suspended Stacking-Faults-Free InAs Nanowires. *Nano Lett.* **10**, 3439–3445 (2010).
 - ¹⁸ Solanki, H. S. *et al.* Tuning mechanical modes and influence of charge screening in nanowire resonators. *Phys. Rev. B* **81**, 115459 (2010).
 - ¹⁹ Octavio, M., Tinkham, M., Blonder, G. E. & Klapwijk, T. M. Subharmonic energy-gap structure in superconducting constrictions. *Phys. Rev. B* **27**, 6739–6746 (1983).
 - ²⁰ Douglass, D. H. Magnetic Field Dependence of the Superconducting Energy Gap. *Phys. Rev. Lett.* **6**, 346–348 (1961).
 - ²¹ de Gennes, P. & Saint-James, D. Elementary excitations in the vicinity of a normal metal-superconducting metal contact. *Phys. Lett.* **4**, 151 – 152 (1963).
 - ²² Ingerman, A., Johansson, G., Shumeiko, V. S. & Wendin, G. Coherent multiple Andreev reflections and current resonances in SNS quantum point contacts. *Phys. Rev. B* **64**, 144504 (2001).
 - ²³ Dayem, A. H. & Grimes, C. C. Microwave emission from superconducting pointcontacts. *Appl. Phys. Lett.* **9**, 47–49 (1966).
 - ²⁴ Landau, L. D. & Lifshitz, M. E. *Theory of Elasticity*, vol. 7 of *Course of Theoretical Physics* (Pergamon Press, 1981), second edn.
 - ²⁵ Mariager, S. O. *et al.* Direct Observation of Acoustic Oscillations in InAs Nanowires. *Nano Lett.* **10**, 2461–2465 (2010).
 - ²⁶ Rosenbaum, J. *Bulk Acoustic Wave Theory and Devices* (Artech House, Inc., 1988).
 - ²⁷ Xin, J., Zheng, Y. & Shi, E. Piezoelectricity of zinc-blende and wurtzite structure binary compounds. *Appl. Phys. Lett.* **91**, 112902 (2007).
 - ²⁸ Mariani, E. & von Oppen, F. Electron-vibron coupling in suspended carbon nanotube quantum dots. *Phys. Rev. B* **80**, 155411 (2009).
 - ²⁹ Sapmaz, S., Jarillo-Herrero, P., Blanter, Y. M., Dekker, C. & van der Zant, H. S. J. Tunneling in Suspended Carbon Nanotubes Assisted by Longitudinal Phonons. *Phys. Rev. Lett.* **96**, 026801 (2006).
 - ³⁰ Leturcq, R. *et al.* Franck-Condon blockade in suspended carbon nanotube quantum dots. *Nat. Phys.* **5**, 327–331 (2009).

Supplementary Information for The self-actuating InAs nanowire-based nanoelectromechanical Josephson junction

Andrey V. Kretinin,^{1,*} Anindya Das,¹ and Hadas Shtrikman¹

¹*Weizmann Institute of Science, Condensed Matter Physics Department, Rehovot, Israel*

- I. CONTACT TRANSPARENCY
- II. MAGNETIC AND TEMPERATURE DEPENDENCE OF THE CRITICAL CURRENT
- III. SIMPLE MODEL OF THE JOSEPHSON JUNCTION COUPLED TO AN EXTERNAL RESONATOR
- IV. SPATIALLY AVERAGED STRAIN ϵ IN THE CASE OF AN ASYMMETRIC NANOWIRE DEVICE
- V. ANOTHER DEVICE USED IN THE EXPERIMENT

I. CONTACT TRANSPARENCY

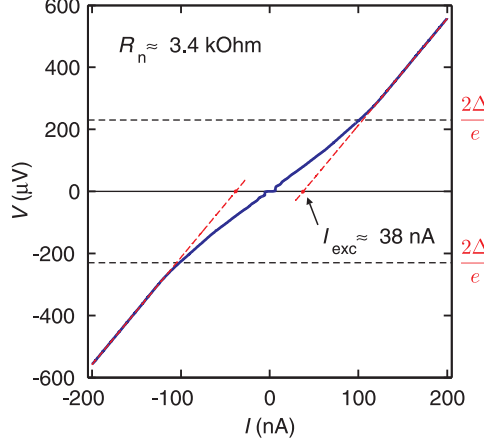


FIG. 1. The excess current of the InAs nanowire Josephson junction described in the main text taken at $V_g = 12.3$ V.

To assess the transparency of the superconducting Al contacts made to the InAs nanowire we measured the so-called excess current¹ I_{exc} . The excess current of the Josephson junction is related to the presence of Andreev Reflections, and defined by the average strength Z of the interface barrier between the normal weak-link and the superconducting contact. The value of I_{exc} can be determined as an intersection of the $I - V$ curve taken for $V > \pm 2\Delta/e$, and extrapolated down to $V = 0$ as shown in Fig. 1. Using this method we found that $I_{\text{exc}} \approx 38$ nA at $V_g = 12.3$ V and the normalised excess current $\frac{R_n I_{\text{exc}}}{e\Delta}$ to be about 1.15, which corresponds to $Z \sim 0.3$ (see Fig. 6 in Ref. 1). Hence, the contact transparency defined as $(1 + Z^2)^{-1}$ is about 90%.

II. MAGNETIC AND TEMPERATURE DEPENDENCE OF THE CRITICAL CURRENT

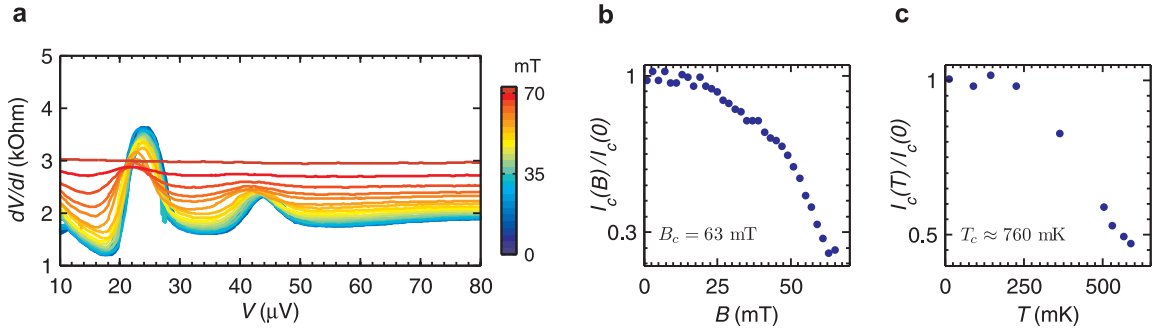


FIG. 2. Additional data on the magnetic field and temperature dependence of dV/dI and I_c for the nanowire device described in the main text.

Figure 1a shows the zoomed in plot of dV/dI as a function of V at different magnetic field shown in Fig. 2a of the main text. The background resistance increasing with the magnetic field made it difficult to reliably extract the position of the resonances. However, it is clear from the plot that the resonance position is virtually independent of the magnetic field. Figure 2b is the plot of the critical current I_c as a function of the magnetic field B measured at $T = T_{\text{base}}$ and $V_g = 12.3$ V, and Fig. 2c is the critical current I_c as a function of the temperature T measured at $B = 0$ and $V_g = 12.3$ V.

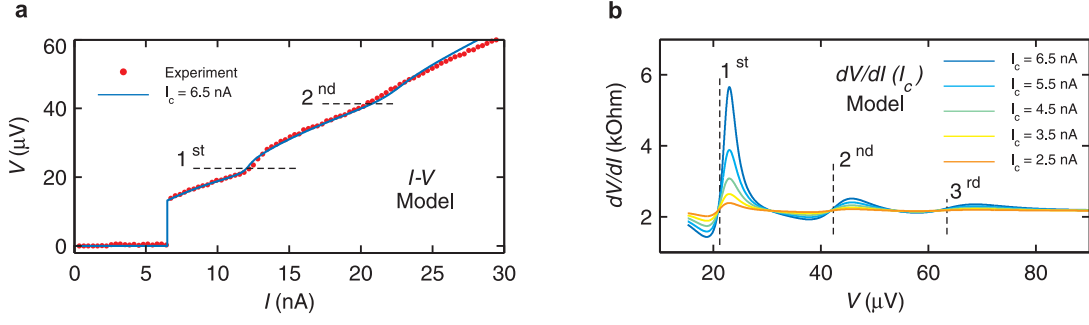


FIG. 3. **Simple model of the underdamped Josephson junction coupled to an external electromagnetic resonator**². (a) The theoretical $I - V$ curve (blue) and experimental data (red circles) taken at $T = T_{\text{base}}$. (b) The theoretical differential resistance dV/dI as a function of V derived from the junction $I - V$ characteristics simulated for different values of I_c . The plot clearly shows that the position of the resonance marked by vertical dashed lines corresponds to the intersection point of curves taken at different I_c .

III. SIMPLE MODEL OF THE JOSEPHSON JUNCTION COUPLED TO AN EXTERNAL RESONATOR

To verify the assumption made in the main text that the position of the resonance is given by the interception of the curves measured at different temperature we used a simple theoretical model of the underdamped Josephson junction weakly coupled to an external electromagnetic resonator.² Here the theoretical $I - V$ curve (Fig. 3a) is the superposition of the $I - V$ curve of the underdamped Josephson junction $V = R_n I$ and three current peaks δI with Lorentzian lineshape $\delta I(V_r) = 0.5zI_c(1 + \xi^2)^{-1}$, where $z \sim 0.5$ is the coupling coefficient, $\xi = 2Q(V/V_r - 1)$, and $Q \sim 3$ is the quality factor. These peaks are caused by the resonant coupling of the a.c.-Josephson oscillations to the external resonator characterised by the resonant voltage V_r and the quality factor Q . To account the effect of the temperature and magnetic field we assumed that the only way these parameters affect the $I - V$ curve is through changing critical current I_c as illustrated in Fig. 2b and Fig. 2c. Figure 3b shows the differential resistance dV/dI derived from the theoretical $I - V$ curve. It is clear that the position of the resonance V_r corresponds to the intersection point of the curves with different I_c , which confirms our assumption.

It is important to note that the Bulk Acoustic Resonator has two distinct resonant frequencies.³ The first one is at $\omega_r = \pi v_a/L$, where $Z(\omega_r) \rightarrow \infty$, which corresponds to the resonance of a parallel LC -circuit. Another one occurs at $\omega_r = v_a/L [\pi^2 - 8k^2]$, where $Z(\omega_r) \rightarrow 0$, and it corresponds to the resonance of a series LC -circuit. The later one was not observed in our experiment, presumably, because the Josephson junction is already strongly underdamped by the relatively large value of C_j , and the additional shunting of the a.c.-Josephson current does not take any visible effect on the $I - V$ curve.

IV. SPATIALLY AVERAGED STRAIN S IN THE CASE OF AN ASYMMETRIC NANOWIRE DEVICE

As mentioned in the main text, the non-zero spatially averaged mechanical strain forbids the appearance of the even resonant modes of BAR. Indeed, the displacement current through the piezoelectric capacitor is $I_D = C_j[\dot{V} - (e_{33}/\epsilon)\dot{S}]$,^{4,5} where e_{33} is the piezoelectric constant, ϵ is the dielectric constant, $S = \langle \partial U(z)/\partial z \rangle$ is the spatially averaged mechanical strain ($U(z)$ is displacement, z is the coordinate along the piezoelectric media), and the dot denotes the time derivative. The second term in the expression is the piezoelectric contribution, which is non-zero when the media accommodates an odd standing acoustic wave. Assuming that the displacement $U(z) \propto \cos(k_n z)$,⁴ where $k_n = \pi n/L$, its spatial average is defined as

$$S = \left\langle \frac{\partial U(z)}{\partial z} \right\rangle = \frac{1}{L} \int_0^L \frac{\partial U(z)}{\partial z} dz \propto \frac{1}{L} \int_0^L \sin\left(\frac{\pi n z}{L}\right) dz, \quad (1)$$

thus this integral is non-zero only for odd standing waves (odd values of n).

However, due to the self aligned geometry of our suspended nanowire device the distance l between ohmic contacts is smaller than the distance L between clumped nanowire ends and the position of their centres is slightly shifted with respect to each other (Fig. 4a). This shift (~ 25 nm) results from the finite accuracy of the e-beam lithography alignment. In this situation the averaging with integral (1) should take place only between the ohmic contacts along the length l (from z_1 to z_2) as shown in Fig. 4b. For purely illustrative purpose we assume that $\partial U/\partial z(z = 0, L) = 0$.

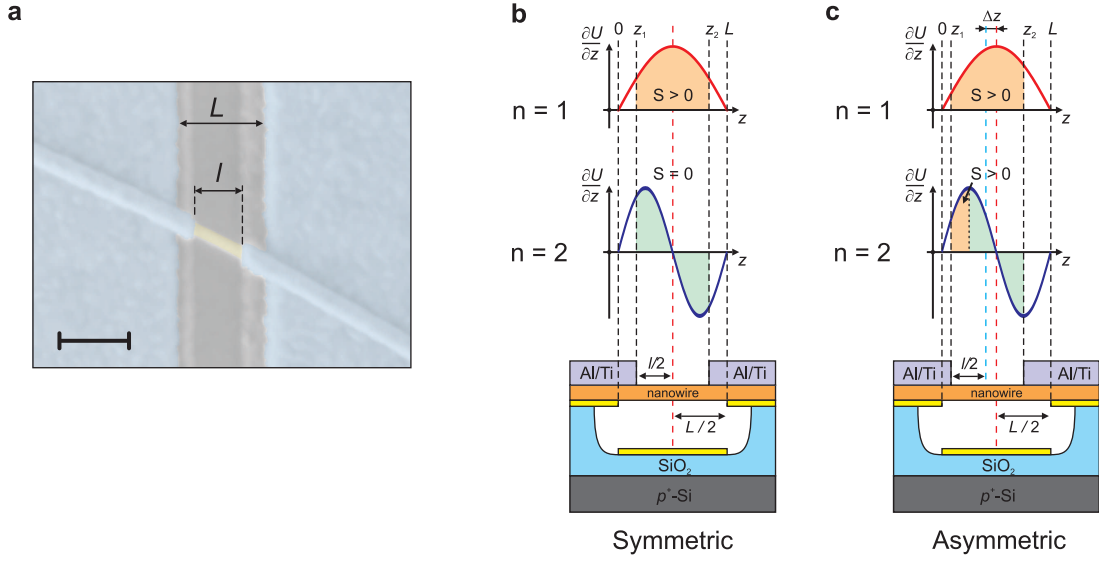


FIG. 4. The asymmetric geometry of the experimental nanowire device and the non-zero spatially averaged strain S . (a) The scanning electron microscope image of a typical device, which shows the difference in mechanical L and electrical l length of the nanowire device. Also, the asymmetry due to the lithography misalignment is clearly visible. The scale bar corresponds to 200 nm. (b) The schematically represented device cross section and the mechanical strain distribution along the nanowire for the first two acoustic modes in the case of the symmetrically positioned contacts. The shaded areas under the strain distribution curves give the value of the integral (1). (c) The same as (b), but with the contacts being asymmetrically positioned with respect to the centre of the nanowire (shifted by Δz). The resulting non-zero values of the integral (1) is shown for the case of $n = 2$.

For the symmetric arrangement of the contacts the first mode gives the non-zero value of S and zero value for the second mode. In the asymmetric case (Fig. 4c), the first mode still gives the non-zero S . Apart from that, the difference Δz between the position of the actual nanowire centre and the centre of the contacted segment makes the spatially averaged strain for the second mode non-zero as well. A similar approach is used to activate even acoustic resonances in the so-called Composite Bulk Acoustic Resonators.⁶⁻⁸

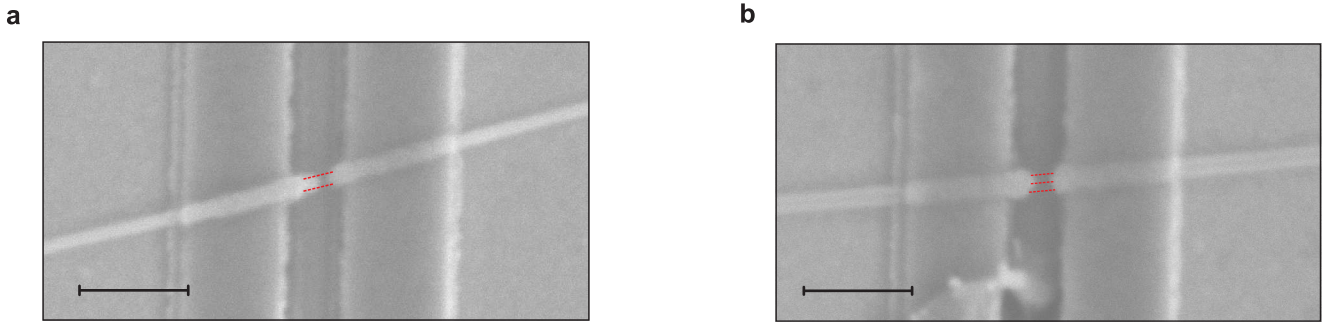


FIG. 5. The scanning electron microscope images of the device described in the main text (a), and additional device described here (b). The scale bar corresponds to 500 nm. During the preparation for the SEM imaging both of the devices were broken down by an unintentional electrostatic discharge. The missing segments of the nanowire are marked by the red lines.

V. ANOTHER DEVICE USED IN THE EXPERIMENT

Apart from the device described in the main text and shown in Fig. 5a we also measured a more complex nanowire configuration, namely two thinner (30 nm in diameter) InAs nanowires held to each other side by side by the Van der Waals forces as shown in Fig. 5b. Both of the nanowires were suspended across the predefined trench and contacted in parallel with Ti/Al contacts, so they form a single weak link of the Josephson junction.

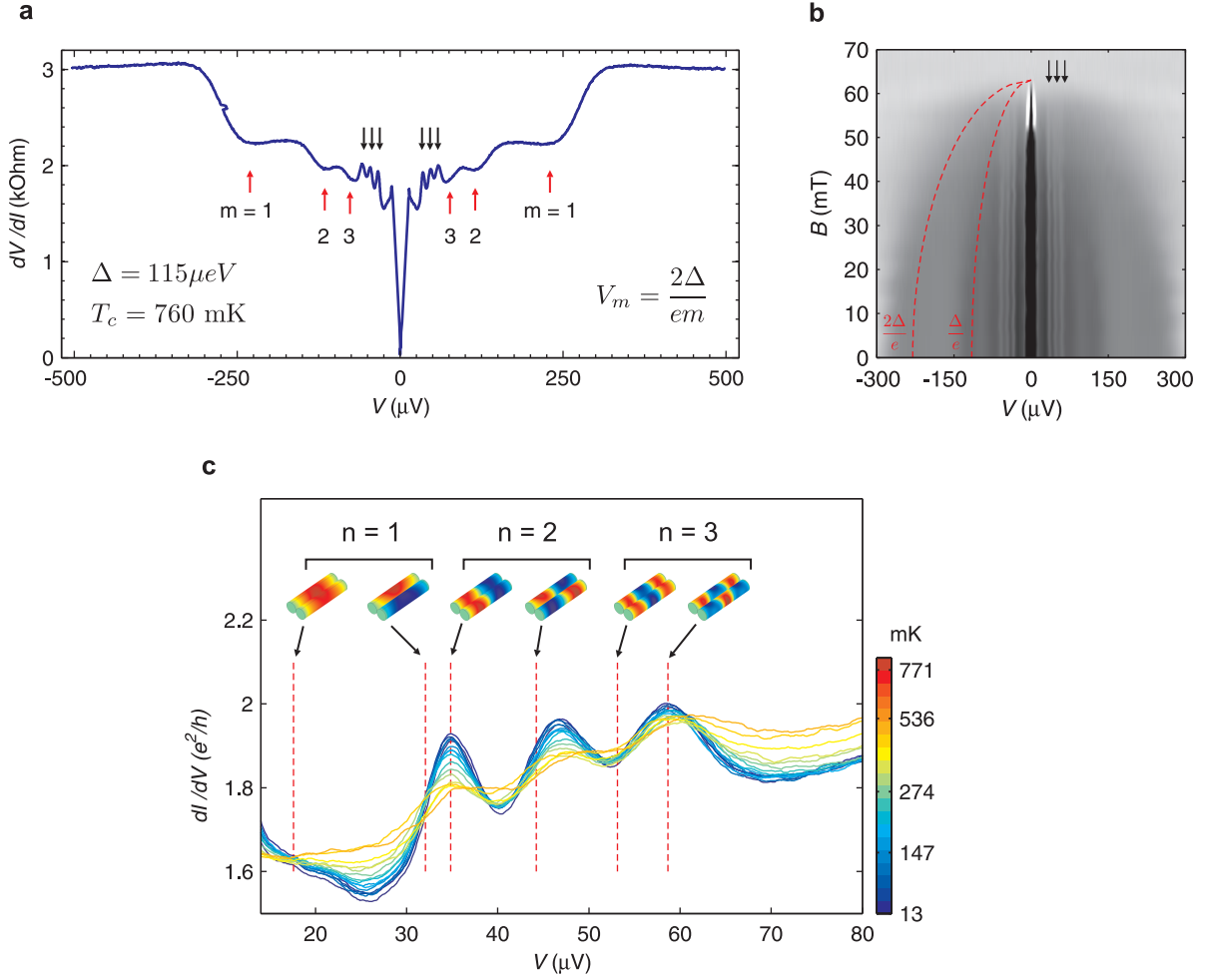


FIG. 6. Additional experimental data obtained from a double beam nanowire device shown in Fig. 5b. **(a)** The differential resistance dV/dI as a function of the voltage V taken at $V_g = 0$ V and $T = T_{\text{base}}$. The red arrows show first three orders of MAR at voltage V_m . The position of the first MAR signature ($m = 1$) gives the superconducting gap $\Delta \approx 115 \mu\text{eV}$ and the estimate for $T_c = 2\Delta/(3.52 k_B) \approx 760$ mK. The black arrows mark the resistance resonances caused by the acoustic wave resonance in double beam system. **(b)** The gray-scale plot of dV/dI made in the $V - B$ plane at $T = T_{\text{base}}$. The red dashed curves show the position of the first two orders of MAR expected from the Landau-Ginzburg theory,⁹ $\Delta(B)/\Delta(0) = \sqrt{1 - (B/B_c)^2}$, where $B_c = 63$ mT is the critical field. The black arrows mark the magnetic field-independent position of the resistance resonances. The position of the resistance resonances stays unchanged while the peak amplitude decreases while B approaches its critical values B_c . **(c)** The zoomed-in plot of the dV/dI resonance taken at different temperatures and zero magnetic field. Identically to the magnetic field dependence shown in **(b)**, the position of the resonances is independent of the temperature. The vertical dashed lines mark the voltage which corresponds to the first three longitudinal harmonics expected for the double InAs beam system with length 230 nm, diameter 30 nm and speed of sound $v_a = 4.5 \cdot 10^3$ m/s. The coloured scale bar refers only to the dV/dI traces taken at different temperature. **(Inset)** The schematically shown submodes of double beam system. The colour scale corresponds to the value of the spatially distributed strain inside each of the beam (red is maximum, blue is minimum). It is clear that the peak in the resistance appears to be closer to the resonance of the submode given by the antisymmetric combination of the main mode.

The differential resistance dV/dI as a function of the bias V taken at $V_g = 0$ V and $T = T_{\text{base}}$ is shown in Fig. 6a. As can be seen from the plot, apart from the MAR signatures with $m = 1, 2, 3$ (red arrows in Fig. 6a) the dV/dI data also shows three closely spaced peak-like features in the range of V between $30 \mu\text{V}$ and $70 \mu\text{V}$ (black arrows in Fig. 6a). Similarly to the single nanowire case described in the main text, the position of these features is independent of magnetic field and temperature as shown in Fig. 6b and 6c. To evaluate the frequency of mechanical resonances of such double beam system we used numerical simulation made with COMSOL Multiphysics Package. We found that every acoustic mode turns out to be splitted into two submodes each of which is a symmetric or antisymmetric linear combination of a single beam acoustic mode (inset in Fig. 6c). Comparing the obtained frequencies with the position of the peaks in dV/dI we concluded that their position corresponds to the antisymmetric submodes for $n = 1, 2, 3$.

However, a more detailed theoretical study is needed to understand why only antisymmetric combination of the main modes are visible in the experiment.

* Present address: School of Physics and Astronomy University of Manchester, Manchester, UK e-mail: andrey.kretinin@manchester.ac.uk

¹ Blonder, G. E., Tinkham, M. & Klapwijk, T. M. Transition from metallic to tunneling regimes in superconducting micro-constrictions: Excess current, charge imbalance, and supercurrent conversion. *Phys. Rev. B* **25**, 4515–4532 (1982).

² Likharev, K. K. *Dynamics of Josephson Junctions and Circuits* (Gordon and Breach Science Publishers, 1986).

³ Rosenbaum, J. *Bulk Acoustic Wave Theory and Devices* (Artech House, Inc., 1988).

⁴ Geller, M. R. & Cleland, A. N. Superconducting qubits coupled to nanoelectromechanical resonators: An architecture for solid-state quantum-information processing. *Phys. Rev. A* **71**, 032311 (2005).

⁵ Trees, B. R., Natu, S. & Stroud, D. Nanomechanical-resonator-induced synchronization in Josephson junction arrays. *Phys. Rev. B* **72**, 214524 (2005).

⁶ Rosenbaum, J., Salvo, J., H.L. & Krishnaswamy, S. Overtone Response of Composite Bulk Acoustic Resonators. In *40th Annual Symposium on Frequency Control*. 1986, 206 – 210 (1986).

⁷ Zhang, Y., Wang, Z. & Cheeke, J. Resonant spectrum method to characterize piezoelectric films in composite resonators. *Ultrasonics, Ferroelectrics and Frequency Control, IEEE Transactions on* **50**, 321 – 333 (2003).

⁸ Pang, W., Zhang, H., Ruby, R. C., Yu, H. & Kim, E. S. Analytical and experimental study on the second harmonic mode response of a bulk acoustic wave resonator. *Journal of Micromechanics and Microengineering* **20**, 115015 (2010).

⁹ Douglass, D. H. Magnetic Field Dependence of the Superconducting Energy Gap. *Phys. Rev. Lett.* **6**, 346–348 (1961).